Draft version May 20, 2016
Preprint typeset using LaTeX style emulateapj v. 08/22/09

MATCHING LYα ABSORPTION TO NEARBY GALAXY HALOS WITH A LIKELIHOOD-BASED METHOD

David M. French, Bart P. Wakker
Department of Astronomy, University of Wisconsin - Madison
Draft version May 20, 2016

ABSTRACT

We present initial results from an ongoing large-scale study of the circumgalactic medium in the nearby Universe ($cz \leq 10,000$ km/s), using archival Cosmic Origins Spectrograph (COS) and Space Telescope Imaging Spectrograph (STIS) spectra of background QSOs. This initial sample contains 35 sight lines, yielding 175 Lyα systems, 41 of which we have paired with nearby galaxies. We introduce a likelihood parameter to quantitatively predict the galaxy responsible for measured absorption in a reproducible way. Results from this sample suggest an anti-correlation between Lyα equivalent width (EW) and impact parameter (ρ) when we normalize by galaxy virial radius (R_{vir}). Absorption is detected in excess near galaxies with inclination $> 50°$. We also detect a dichotomy in the equivalent widths of absorption systems around $\Delta v = v_{galaxy} - v_{gas}$, with positive Δv absorption median $EW = 343 \pm 10$ mÅ, and negative Δv absorption median $EW = 124 \pm 9$ mÅ.

Subject headings: IGM, CGM, galaxies

1. INTRODUCTION

It is well known that galaxies must continue to accrete gas throughout their lifetimes in order to sustain observed levels of star formation (e.g. Erb 2008, Putman et al. 2009b). This additional gas must come from the diffuse intergalactic medium (IGM), where the majority of the baryons in the universe reside (Penton et al. 2002, 2004; Lehner et al. 2007; Danforth & Shull 2008; Shull et al. 2012). How exactly this IGM gas eventually falls into the halos and disks of galaxies is still highly uncertain, as observational constraints are hard to come by. Because of the diffuse nature of IGM gas it is most readily and sensitively detected as absorption in the spectra of background active galactic nuclei (AGN). The advent of the sensitive UV spectrographs STIS and COS on the Hubble Space Telescope (HST) has provided a wealth of information on the properties and distribution of both the ions of heavy elements as well as the Lyman series of neutral H I gas around galaxies.

Individual concentrations of gas along a given sightline imprint absorption lines on the spectrum in the direction of the QSO. The metal lines trace the star formation history within the intervening gas, and neutral hydrogen lines (Lyα) indicate both the location and velocities of outflowing gas as well as the presence of fuel for future star formation. Numerous studies using these observations have shown that many Lyα absorbers trace individual galaxy halos (e.g. Wakker & Savage 2009, Danforth et al. 2014, Stocke et al. 2013 & 2014, Liang et al 2014, Lanzetta et al 1995, Chen et al. 1998, 2001a, Tripp et al. 1998, Steidel et al. 2010, Prochaska et al. 2011, Thom et al 2012, Tumlinson et al. 2011 & 2013).

Some recent studies find that about half of Lyα absorbers lie within galaxy haloes, at impact parameters $\rho < 350$ kpc (Côté et al. 2005, Prochaska et al. 2006). In addition, Wakker & Savage (2009) find that an absorber lies within 400 kpc and 400 km/s for 90% of galaxies brighter than $0.1L_*$, and all galaxies have a Lyα absorber within 1.5 Mpc. Higher redshift studies, such as Rudie et al. (2012) at $2 < z < 3$, find evidence for an elevated density of absorbers up to 2 Mpc from galaxies. Wakker & Savage (2009) also confirmed a correlation between Lyα absorption linewidth and impact parameter ρ, observing that the broadest lines (FWHM >150 km/s) are only seen within 350 kpc of a galaxy, while at $\rho > 1$ Mpc, only lines with FWHM < 75 km/s occur. This suggests that the temperature of gas increases in the presence of galaxies.

In addition, studying the enrichment of galaxy halos is necessary for constraining outflow models and informing stellar feedback prescriptions. Directly measuring the velocity field and column densities of absorbers as a function of impact parameter and orientation around galaxies would provide the clearest evidence of inflow or outflow activity, but results are still uncertain. Kacprzak et al. (2011) claim to find that Mg II equivalent widths correlate with galaxy inclination, but Mathes et al. (2014) find no such correlation for Lyα and O VI absorbers. Furthermore, we should expect outflowing gas to be more highly enriched and trace the metallicity of the associated galaxy, with inflowing gas instead appearing only in H I. Both Stocke et al. (2013) and Liang & Chen (2014) find an "edge" to heavy ion absorption at $\sim 0.5R_{vir}$, but with Lyα covering fractions of $\sim 0.75 - 1$ continuing out to R_{vir}. However, Mathes et al. (2014) measures O VI absorption out to $\sim 3R_{vir}$, and Savage et al. (2014) find that more than half of O VI absorption occurs beyond 1 R_{vir}.

Recent results from Kacprzak et al. (2011 & 2012) suggest that absorbing systems have a preferred orientation with respect to the major and minor axes of the galaxies they are associated with. This could be evidence of inflows and outflows, or an effect of the global structure of galaxy halos, but the statistics are not yet good enough to provide consistent answers. A larger-scale study of inclination and azimuthal angles vs. absorber properties is needed in order to elucidate the distribution of absorbing systems around galaxies. This is most easily done for the largest galaxies in the nearby universe, where it is possible to obtain inclinations and unambiguous absorber associations.

Previous studies have suffered from small sample sizes (e.g. Mathes et al. 2014 use 14 galaxies, Stocke et al. 2013 use 11, Werk et al. 2014 use 44), and incompleteness due to their higher mean redshifts (e.g. the Mathes et al. 2014 sample is $0.12 < z < 0.67$, and Werk et al. 2014 are complete to $\sim L^*$ at $z \sim 0.2$). To address these shortcomings, we are conducting a large survey of the properties of intergalactic gas in the nearby universe, where we have good and relatively complete information on both faint and bright galaxies, in order to reveal how the IGM and galaxies affect each other. We are taking advantage of the over 500 archived QSO and Seyfert spectra taken by the Cosmic Origins Spectrograph (COS) and Space Telescope Imaging Spectrograph (STIS) on the Hubble Space Telescope (HST), combined with the wealth of information available for the $\sim 100,000$ galaxies with $cz < 10,000$ km/s found in the NASA Extragalactic Database (NED) to probe the environment of absorbing gas systems in the nearby universe. This approach allows for an unbiased understanding of the distribution of the gas around galaxies, which requires looking for both detections and non-detections of gas, both near as well as far away from galaxies.

This paper presents initial results from our pilot study of 35 sight lines, chosen for their proximity to large galaxies and high S/N ratios. This paper is organized as follows: in Section 2 we present the data and analysis techniques, in Section 3 we present the results, and in Section 4 we discuss possible interpretations of our results.

2. DATA AND ANALYSIS

2.1. *Galaxy Data*

The goal of this study relies on knowing the locations and properties of all galaxies near to detected Lyα absorption lines. To facilitate this, we have constructed a dataset of all $z \leq 0.033$ ($cz \leq 10,000$ skm/s) galaxies with published data available through the NASA Extragalactic Database (NED[1]). This dataset contains over 108,000 entries, and includes data from SDSS, 2MASS, 2dF, 6dF, RC3, and many other, smaller surveys. Our criteria for including a galaxy in this dataset is only an accurate, spectroscopic redshift which places the galaxy in the $cz \leq 10,000$ km/s velocity range. This restriction leads to a completeness limit of $B \lesssim 18.7$ mag, or $\sim 0.2L_*$, at $cz = 10,000$ km/s, and progressively better towards lower velocities (see Figure 1). This limit will vary some depending on which major surveys include a particular region of the sky.

In addition, we have homogenized the galaxy data beyond the steps taken by NED by normalizing all measurements of galaxy inclination, position angle, and diameter to 2MASS K-band values. Most galaxies in NED have measures of inclination, position angle and diameter available in several different bands, so in order to make meaningful comparisons it is necessary to automatically choose one band for all measurements. We chose 2MASS values for this because it was an all-sky survey, and represents the largest fraction of available galaxy data. Physical galaxy diameters are derived from 2MASS

[1] This research has made use of the NASA/IPAC Extragalactic Database (NED) which is operated by the Jet Propulsion Laboratory, California Institute of Technology, under contract with the National Aeronautics and Space Administration.

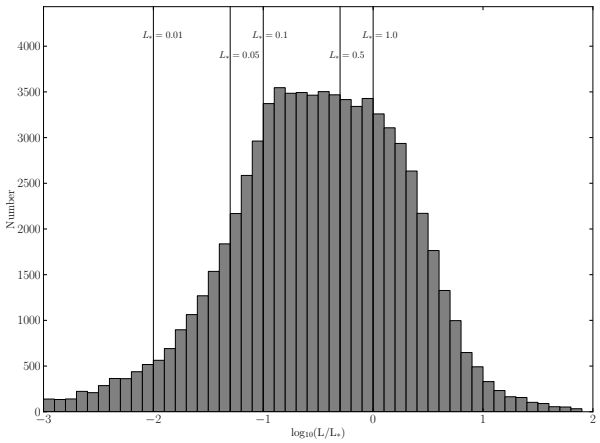

Figure 1. Distribution of L/L_* values for all galaxies in the dataset. Black vertical lines highlight 1, 0.5, 0.1, 0.05 and 0.01 L_*. The turnoff around $0.1L_*$ shows that on average, the dataset is complete to $0.1L_*$.

K_s "total" angular diameter measurements and galaxy distances. 2MASS K_s "total" diameter estimates are surface brightness extrapolation measurements and are derived as

$$r_{tot} = r' + a(ln(148)^b, \quad (1)$$

where r_{tot} is defined as the point where the surface brightness extends to 5 disk scale lengths, r' is the starting point radius ($> 5" - 10"$ beyond the nucleus, or core influence), and a and b are Sersic exponential function scale length parameters ($f = f_0 \exp(-r/a)^{(1/b)}$, see Jarret et al. 2003 for a full description). Approximately 50% of all the galaxies have this 2MASS K_s "total" diameter. Of the remainder, 20% have SDSS diameters, 27% have no published diameter, and 3% have diameters from other surveys. We convert values in these other bands to 2MASS K_s "total" diameters via a simple least squares linear fit when necessary. **NEEDS TO BE CHECKED FOR FULL SKY**

We used B-band magnitudes to estimate each galaxy's luminosity as a ratio of L_* as follows:

$$\frac{L}{L_*} = 10^{-0.4(M_B - M_{B_*})}. \quad (2)$$

We adopt the CfA galaxy luminosity function by Marzke et al. (1994), which sets B_* = -19.57. Direct B band measurements are available for $\sim$ 30% of galaxies, and most of the rest have SDSS g and r magnitudes, which can be converted to B via $B = g + 0.39(g-r) + 0.21$ (Jester et al. 2005). Finally, we also compute an estimate of the virial radius of each galaxy as $logR_{vir} = 0.69logD + 1.24$. This follows the parametrization of Stocke et al. (2013) relating a galaxy's luminosity to its virial radius, and the Wakker & Savage (2009) empirical relation between diameter and luminosity (see Wakker et al. 2015 and references therein for further details).

This homogeneous galaxy data table allows us to draw direct comparisons between the properties of the absorbers and the properties, separations, and environments of nearby galaxies with unprecedented complete-

Target	R.A.	Dec.	z	Program	Grating	Obs ID	Obs Date	T_{exp} [ks]	S/N
1H0717+714	07 21 53.3	+71 20 36	0.5003	12025	G130M	LBG812	2011 12 27	6.0	37
1H0717+714	07 21 53.3	+71 20 36	0.5003	12025	G160M	LBG812	2011 12 27	8.3	31
2dFGRS_S393Z082	02 45 00.8	-30 07 23	0.3400	12988	G130M	LC1045	2013 05 27,28	17.7	11
2dFGRS_S393Z082	02 45 00.8	-30 07 23	0.3400	12988	G130M	LC1040	2013 05 28,29	17.7	11
3C273.0	12 29 06.7	+02 03 08	0.1583	12038	G130M	LBGL31	2012 04 22	4.0	110
3C351.0 (STIS)	17 04 41.4	+60 44 31	0.3719	8015	E140M	O57901	1999 06 27	77.0	10
3C66A	02 22 39.6	+43 02 08	0.4440	12612	G130M	LBXC04	2012 11 1	12.6	24
3C66A	02 22 39.6	+43 02 08	0.4440	12863	G160M	LC0J01	2012 11 8	7.2	15
CSO395	12 11 14.6	+36 57 39	0.1690	12248	G130M	LBH062	2011 04 27	3.0	11
CSO395	12 11 14.6	+36 57 39	0.1690	12248	G160M	LBH062	2011 04 27	4.8	9
H1101-232	11 03 37.7	-23 29 31	0.1860	12025	G130M	LBG804	2011 07 5,6	13.3	16
H1101-232	11 03 37.7	-23 29 31	0.1860	12025	G160M	LBG804	2011 07 5,6	13.3	10
HE0238-1904	02 40 32.6	-18 51 51	0.6310	11541	G130M	LB6804	2009 12 31	14.4	36
HE0238-1904	02 40 32.6	-18 51 51	0.6310	11541	G160M	LB6804	2009 12 31	7.5	22
HE1228+0131	12 30 50.0	+01 15 21	0.1170	11686	G130M	LB4F09	2011 07 7	11.0	61
HE1228+0131	12 30 50.0	+01 15 21	0.1170	11686	G160M	LB4F10	2011 07 20,21	11.0	44
HS0624+6907 (STIS)	06 30 02.6	+69 05 03	0.3700	9184	E140M	06E11	2002 01 2	62.0	6
HS0624+6907 (STIS)	06 30 02.6	+69 05 03	0.3700	9184	E140M	06E11	2002 02 23,24	62.0	8
IRAS_Z06229-6434	06 23 07.7	-64 36 19	0.1289	11692	G130M	LB3J09	2009 12 19	8.7	25
IRAS_Z06229-6434	06 23 07.7	-64 36 19	0.1289	11692	G160M	LB3J58	2010 09 15	8.0	18
MRK1014	01 59 50.2	+00 23 41	0.1630	12569	G130M	LBP404	2012 01 25	1.8	17
MRK290	15 35 52.3	+57 54 09	0.0296	11524	G130M	LB4Q02	2009 10 28	3.9	38
MRK290	15 35 52.3	+57 54 09	0.0296	11524	G160M	LB4Q02	2009 10 28	4.8	18
MRC2251-178	22 54 05.9	-17 34 55	0.0661	12029	G130M	LBGB03	2011 09 29	4.6	38
MRC2251-178	22 54 05.9	-17 34 55	0.0661	12029	G160M	LBGB03	2011 09 29	5.4	26
PG0003+158	00 05 59.3	+16 09 49	0.4509	12038	G130M	LBGL17	2011 10 22	10.4	24
PG0003+158	00 05 59.3	+16 09 49	0.4509	12038	G160M	LBGL17	2011 10 22	10.9	20
PG1121+423	11 24 39.2	+42 01 45	0.2340	12024	G130M	LBG703	2011 04 25	5.0	20
PG1121+423	11 24 39.2	+42 01 45	0.2340	12024	G160M	LBG703	2011 04 25	5.8	14
PG1211+143 (STIS)	12 14 17.7	+14 03 13	0.0804	8571	E140M	061Y0	2002 02 4,5,6,7,8	67.4	19
PG1216+069	12 19 20.9	+06 38 38	0.3313	12025	G130M	LBG881	2012 02 4,5	5.1	23
PG1216+069	12 19 20.9	+06 38 38	0.3313	12025	G160M	LBG881	2012 02 4,5	5.6	16
PG1302-102	13 05 33.0	-10 33 20	0.2784	12038	G130M	LBGL04	2011 08 16	6.0	28
PG1302-102	13 05 33.0	-10 33 20	0.2784	12038	G160M	LBGL04	2011 08 16	6.9	33
PG1307+085	13 09 47.0	+08 19 47	0.1550	12569	G130M	LBP411	2012 06 16	1.8	19
PG1626+554	16 27 56.2	+55 22 32	0.1330	12029	G130M	LBGB01	2011 06 15	3.3	26
PG1626+554	16 27 56.2	+55 22 32	0.1330	12029	G160M	LBGB01	2011 06 15	4.3	18
PKS2005-489	20 09 25.4	-48 49 53	0.0710	11520	G130M	LB4R03	2009 09 21	2.5	22
PKS2005-489	20 09 25.4	-48 49 53	0.0710	11520	G160M	LB4R03	2009 09 21	1.9	13
RBS1795	21 54 51.0	-44 14 05	0.3440	11541	G130M	LB6809	2010 06 23	8.2	26
RBS1795	21 54 51.0	-44 14 05	0.3440	11541	G160M	LB6809	2010 06 23,24	8.5	17
RBS2070	23 59 07.8	-30 37 39	0.1650	12864	G130M	LC0F01	2013 06 15,19	17.0	16
RX_J0714.5+7408	07 14 36.2	+74 08 11	0.3710	12275	G130M	LBH402	2011 03 18	8.3	18
RX_J1330.8+3119	13 30 53.2	+31 19 32	0.2410	12248	G130M	LBHO85	2011 07 11	4.3	11
RX_J1330.8+3119	13 30 53.2	+31 19 32	0.2410	12248	G160M	LBHO85	2011 07 11	6.8	11
RX_J1503.2+6810	15 03 16.5	+68 10 06	0.1140	12276	G130M	LBI609	2010 12 31	1.9	11
SBS1108+560	11 11 32.1	+55 47 25	0.7650	12025	G130M	LBG809	2011 05 12	8.4	4
SBS1108+560	11 11 32.1	+55 47 25	0.7650	12025	G160M	LBG809	2011 05 12	8.8	14
SBS1122+594	11 25 53.7	+59 10 22	0.8580	11520	G130M	LB4R11	2009 11 07	9.9	14
SBS1122+594	11 25 53.7	+59 10 22	0.8580	11520	G160M	LB4R11	2009 11 07	10.5	12
SBS1503+570	15 04 55.6	+56 49 20	0.3589	12276	G130M	LBI617	2011 10 19	5.2	11
SBS1537+577	15 38 10.0	+57 36 13	0.0734	12276	G130M	LBI606	2011 10 19	5.2	12
SDSSJ080838.80+051440.0	08 08 38.8	+05 14 40	0.3610	12603	G130M	LBS330	2012 03 17	4.7	8
SDSSJ080908.13+461925.6	08 09 08.1	+46 19 26	0.6563	12248	G130M	LBHO77	2010 10 06	3.1	14
SDSSJ080908.13+461925.6	08 09 08.1	+46 19 26	0.6563	12248	G160M	LBHO77	2010 10 06	5.0	13
SDSSJ135341.03+361948.0	13 53 41.0	+36 19 48	0.1470	13444	G130M	LC8L04	2014 06 14	10.2	18
SDSSJ140428.30+335342.0	14 04 28.3	+33 53 42	0.5490	12603	G130M	LBS320	2013 03 03	7.7	8
TON488	10 10 00.7	+30 03 21	0.2564	12025	G130M	LBG810	2011 05 19	10.8	17
TON488	10 10 00.7	+30 03 21	0.2564	12025	G160M	LBG811	2011 05 21	10.8	17
TON1009	09 09 06.1	+32 36 31	0.8090	12603	G130M	LBS328	2012 04 22	4.7	11

Table 1
Observations.

ness. The full dataset will be publicly released and discussed in further detail in a forthcoming paper (French et al. 2016, in prep).

2.2. *Spectra*

This initial pilot study contains 35 sightlines to bright QSOs observed with COS (32 of 35) and STIS (3 of 35). We chose sightlines by first sorting the galaxy data table described above by galaxy diameter. This sorted list is then correlated with the full list of publicly available sightlines, and only those systems with impact parameter less than 500 Mpc are kept. Finally, we reject any messy, overly complicated, or low S/N sightlines and select the top 35 (again, sorted by galaxy diameter).

All COS spectra for the target sightlines were obtained through the Barbara A. Mikulski Archive for Space Telescopes (MAST), and processed with CALCOS v3.0. We combined individual exposures by the method of Wakker et al. (2015), which corrects the COS wavelength scale by cross-correlating all ISM and IGM lines in each exposure. This method addresses the up to ±40 km/s misalignments produced by CALCOS, and produces a corrected error array based on Poisson noise, which better matches the measured errors then the errors delivered in the x1d files. We then combine multiple exposure by aligning Galactic absorption lines with 21-cm spectra, and adding up the total counts in each pixel before converting to flux using the original, average flux-count ratio at each wavelength.

The STIS data was processed in the same manner as described in Wakker & Savage (2009), and thus we only give a short summary here. The STIS calibrated fits files were downloaded from MAST, and STIS-E140M echelle orders were combined into a single spectrum. The photon counts and errors were interpolated onto a common grid, counts were added and weighted by the rms at each pixel, and finally converted back to flux. Table 2 summarizes the properties of the selected QSO targets.

3. RESULTS

We have identified 175 Lyα absorption lines in the spectra of our initial 35 QSO sample. Of these, 41 can be unambiguously associated with a single nearby galaxy, 46 are near more than one galaxy, and 88 reside greater than $\rho = 500$ kpc and $\Delta v = 400$ km/s from any galaxy. In order to be considered for a pairing, a galaxy and absorption feature must appear within 400 km/s in velocity and 500 kpc in physical impact parameter from each other. When multiple galaxies pass these criteria for a particular line, we are left with two options. 1) one galaxy is obviously far larger and closer in physical and velocity space to the line, and may have several satellite galaxies, or 2) no single galaxy if obviously dominant, and we do not include this line in further analysis.

To facilitate this decision, we compute the likelihood, $\mathcal{L}$, of every possible galaxy-absorber pairing as follows:

$$\mathcal{L} = Ae^{-(\frac{\rho}{R})^2} e^{-(\frac{\Delta v}{200})^2}. \quad (3)$$

Here ρ is the physical impact parameter, Δv the velocity difference between the absorber and the galaxy ($\Delta v = v_{galaxy} - v_{absorber}$), and A is a factor included to increase the likelihood in the case that $R \geq \rho$ (in which case $A = 2$, otherwise $A = 1$). We compute $\mathcal{L}$ for two different values of R: R_{vir}, the virial radius of the galaxy, and $d^{1.5}$, the major diameter of the galaxy to the power of 1.5. $\mathcal{L}$ computed with R_{vir} is liable to select satellite galaxies instead of the larger hosts, so including a version with $d^{1.5}$ serves as a two-tiered selection system. An absorber-galaxy system separated by 200 km/s in velocity and $1R_{vir}$ would have $\mathcal{L} = 0.27$. In order for an absorber to be marked as "associated" with a particular galaxy, its $\mathcal{L}$ must be a factor of 5 larger than the next best possible association, and $\mathcal{L} \geq 0.001$. We then visually inspect each system before it is included in the final sample, rejecting associations with galaxies residing in complex or group environments.

Figures 2.2 and 2(b) show a clean example of a Lyα absorption line with a map of its galaxy environment, showing an unambiguous pairing between the absorption feature at 4295 km/s toward TON1009 and galaxy IC2439 ($\mathcal{L} = 0.45$). Unless explicitly stated, all following analysis concerns similarly unambiguous "associated" systems.

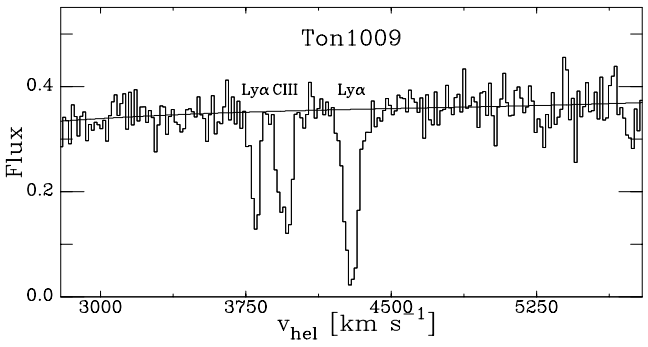

(a)

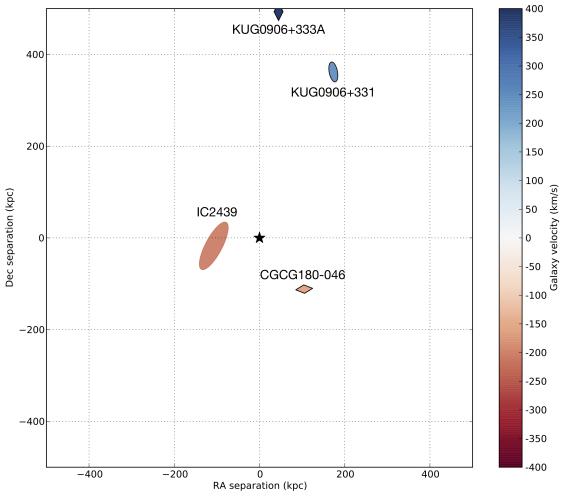

(b)

Figure 2. a) An example Lyα line found in a sightline towards target TON1009 at 4295 km/s. b) A map of *all* galaxies within a 500 kpc impact parameter target TON1009 sightline and with velocity (cz) within 400 km/s of absorption detected at 4295 km/s (central black star). The galaxy IC2439 ($v = 4494$ km/s, inclination $= 71°$) can be unambiguously paired with the Lyα absorption feature at $v = 4295$ km/s because it is the largest and closest galaxy in both physical and velocity space to the absorption feature.

Target	Galaxy	$\mathcal{L}$	R_{vir} [kpc]	ρ (kpc) [kpc]	v_{galaxy} [km/s]	Δv [km/s]	Inc. [deg]	Az. [deg]	$v_{Ly\alpha}$ [km/s]	W$_{Ly\alpha}$ [mÅ]
(1)	(2)	(3)	(4)	(5)	(6)	(7)	(8)	(9)	(10)	(11)
1H0717+714	UGC03804	0.24	173	207	2887	17	53	7	2870	343±6
1H0717+714	UGC03804	0.21	173	207	2887	-69	53	7	2956	39±4
2dFGRS_S393Z082	NGC1097	1.8*	273	112	1271	32	47	12	1239	570±21
3C273.0	NGC4517	0.02	193	365	1128	115	83	72	1013	376±3
3C273.0	NGC4536	0.0018	198	359	1808	-348	65	46	2156	57±2
3C66A	UGC01832	1.7	192	56	5913	-52	65	16	5965	53±6
CSO395	UGC07207	0.87	103	83	1051	85	61	x	966	194±14
CSO395	UGC07207	1.0	103	83	1051	26	61	x	1025	343±15
H1101-232	MCG-04-26-019	0.33	173	179	3623	43	65	26	3580	573±12
HE1228+0131	2MASXJ12303439+0116243	0.18	127	159	9319	80	28	60	9239	249±3
MRC2251-178	MCG-03-58-009	1.4*	319	320	9030	-21	59	39	9051	60±4
MRK290	NGC5987	0.77*	322	486	3010	-95	65	12	3105	511±5
MRK290	NGC5987	0.37*	322	486	3010	-197	65	12	3207	319±4
MRK1014	NGC0768	0.12*	253	486	7021	-59	73	85	7080	117±11
PG0003+158	NGC7814	0.081	171	197	1050	217	65	47	833	131±15
PG0003+158	NGC7814	0.097	171	197	1050	-200	65	47	1250	79±9
PG1121+423	SDSSJ112418.74+420323.1	0.046	104	129	7374	248	65	20	7126	156±7
PG1121+423	SDSSJ112418.74+420323.1	0.17	104	129	7374	95	65	20	7279	46±6
PG1121+423	SDSSJ112418.74+420323.1	0.2	104	129	7374	46	65	20	7328	359±7
PG1216+069	SDSSJ121903.72+063342.9	0.09	71	110	3833	20	61	65	3813	360±10
PG1302-102	NGC4939	0.05*	235	265	3110	-338	46	61	3448	71±5
PG1307+085	CGCG072-007	0.003	193	440	7119	-160	50	43	7279	64±7
RX_J0714.5+7408	UGC03717	0.13*	202	271	4188	114	61	83	4074	58±7
RX_J0714.5+7408	UGC03717	0.15*	202	271	4188	-76	61	83	4264	410±9
RX_J1330.8+3119	UGC08496NED02	0.08	101	160	4829	-10	59	46	4839	413±16
RX_J1330.8+3119	UGC08492	0.081*	204	335	7414	13	16	41	7401	330±15
RX_J1503.2+6810	CGCG318-012	0.031*	250	325	9765	-357	50	1	10122	44±14
SBS1108+560	UGC06225	1.9	228	29	699	-33	77	82	732	1082±82
SBS1108+560	UGC06225	0.53*	228	29	699	-230	77	82	929	284±51
SBS1122+594	NGC3642	0.035	150	226	1588	-208	8	3	1796	29±8
SBS1537+577	SDSSJ153802.75+573018.3	0.33	87	91	3525	-24	80	15	3549	447±28
SDSSJ080838.80+051440.0	UGC04239	0.87*	279	378	8763	23	44	38	8740	883±24
SDSSJ080838.80+051440.0	UGC04239	0.45*	279	378	8763	-164	44	38	8927	130±19
SDSSJ080908.13+461925.6	SDSSJ080842.74+461828.9	0.015	103	133	7092	318	37	4	6774	543±10
SDSSJ080908.13+461925.6	SDSSJ080842.74+461828.9	0.076	103	133	7092	192	37	4	6900	151±10
SDSSJ080908.13+461925.6	SDSSJ080842.74+461828.9	0.19	103	133	7092	-25	37	4	7117	176±12
SDSSJ140428.30+335342.0	KUG1402+341	1.4	204	118	7919	35	69	63	7884	889±28
TON488	UGC05478	0.89	92	58	1378	128	12	x	1250	68±9
TON488	UGC05478	1.3	92	58	1378	3	12	x	1375	452±12
TON1009	NGC2770	0.19*	204	274	1947	-14	78	43	1961	350±21
TON1009	IC2439	1.2	153	109	4299	14	71	51	4285	343±17

Table 2
All associated systems. The largest $\mathcal{L}$ value is given, where a (*) indicates $d^{1.5}$ was used, otherwise the quoted $\mathcal{L}$ was computed with R_{vir}. For all entries, 'x' indicates unknown values.

Additionally, we split the absorber-galaxy catalog based on the velocity difference of the two, Δv. With this scheme, we refer to an absorber with a velocity *lower* than the associated galaxy as *blueshifted*, while an absorber with a velocity *higher* is referred to as *redshifted*. The rest of the results will be analyzed based upon this splitting.

3.1. *EW-ρ Anti-correlation*

Numerous previous studies have suggested that Lyα equivalent width (EW) is anti-correlated with impact parameter (ρ) to the nearest galaxy. We find a weak correlation, as shown in Figure **??**(a). However, we find a stronger anti-correlation when we normalize ρ by R_{vir}. Figure **??**(b) shows this expected anti-correlation when plotting EW vs ρ/R_{vir}. A possible explanation for this trend is that larger galaxies host larger, more physically extent CGM halos. We would thus expect the absorber EW to also correlate positively with R_{vir}. Figure 4 shows EW as a function of R_{vir}, with the blue-dashed and red-dotted lines show the average EW in bins of 50 kpc of R_{vir}. A weak positive correlation is possibly present between EW and R_{vir} for the blueshifted absorbers, but there is little evidence of any correlation for the redshifted sample.

3.2. *Velocity Difference* (Δv)

Additionally, we find evidence for an anti-correlation between absorber EW and the velocity difference between the galaxy and the associated absorption, Δv. The mean and maximal EW of absorption increases with decreasing Δv (see Figure 5). In total, 25/41 (61%) of ab-

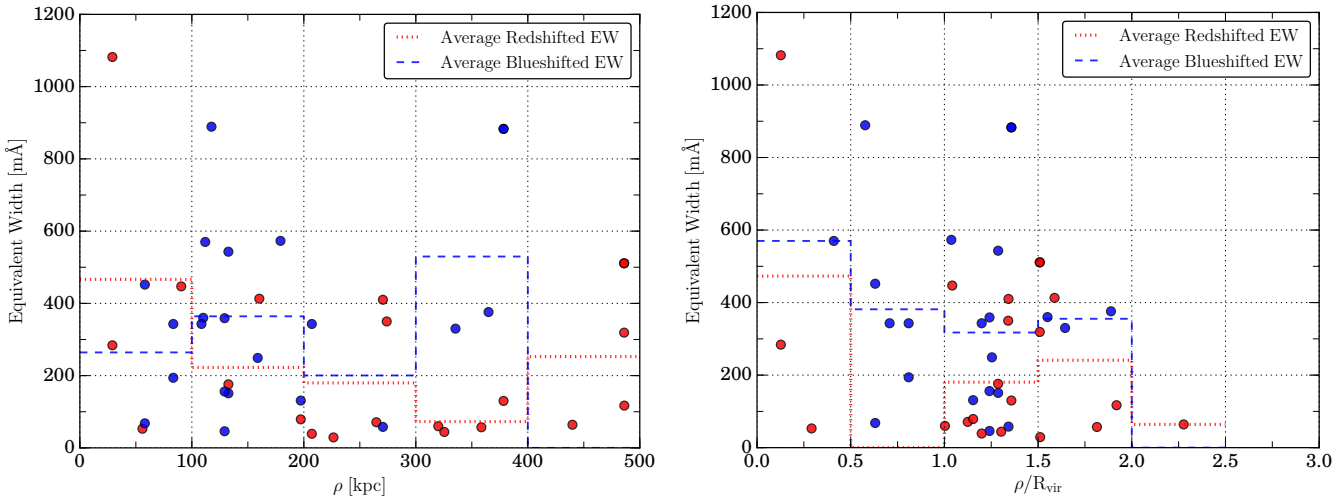

Figure 3. a) Equivalent width of each absorber as a function of impact parameter, ρ (kpc), b) Equivalent width as a function of ρ/R_{vir}. The anti-correlation is strongest when scaling ρ by the galaxy virial radius. Absorbers are separated into red and blue-shifted samples based on Δv. Bins of mean EW are overplotted in red-dashed, and blue-dotted lines for their respective samples.

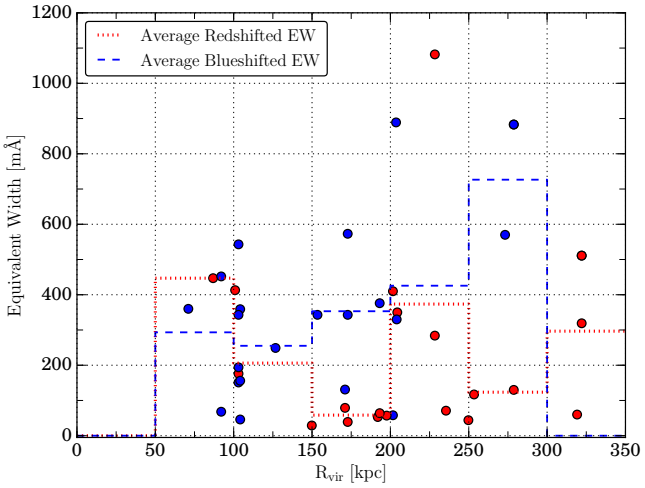

Figure 4. Equivalent width of each absorber as a function of the virial radius of the associated galaxy in the sample. The blue-dotted and red-dashed lines shows the average EW in 50 kpc bins of R_{vir} for the blueshifted and redshifted absorbers, respectively.

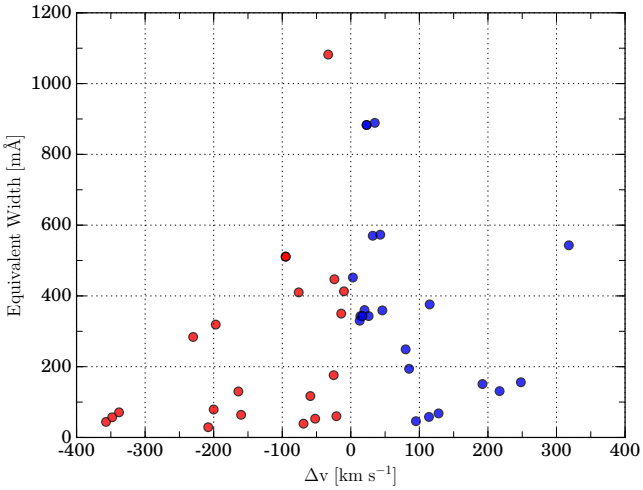

Figure 5. Equivalent width as a function of the velocity separation between the galaxy and absorption line.

sorbers are found within ±100 km/s, and the highest EW absorbers are found within ±50 km/s of their associated galaxy velocities.

3.3. *Inclination*

In this section we examine the inclinations of the associated galaxies compared to the distributions of absorbers. We compute galaxy inclination, i, as follows:

$$\cos(i) = \sqrt{\frac{q^2 - q_0^2}{1 - q_0^2}}, \tag{4}$$

where $q = b/a$, the ratio of the minor to major axis, and q_0 is the intrinsic axis ratio, set to $q_0 = 0.2$ for all galaxies.

Figure 6 shows red and blueshifted absorbers' EW plotted against the inclinations of their associated galaxies. We note that there is an apparent dichotomy between the distributions, where blue shifted absorbers appear around nearly all inclinations of galaxies, but redshifted absorbers appear preferentially near highly-inclined galaxies ($i \geq 50$ deg). In addition, redshifted absorbers appear with lower EW than those blueshifted across all inclinations. The mean EW of all redshifted absorbers is $\overline{EW} = 237 \pm 16$ mÅ, compared to $\overline{EW} = 353 \pm 12$ mÅ for blueshifted absorbers. To test if the distributions of red and blue-shifted absorbers are actually different we performed KS and AD statistical distribution tests, which both yielded p-values = 0.05. While $p = 0.05$ is often quoted as a threshold for significance, we believe a larger sample size is needed before we can claim the presence of a true, physical dichotomy.

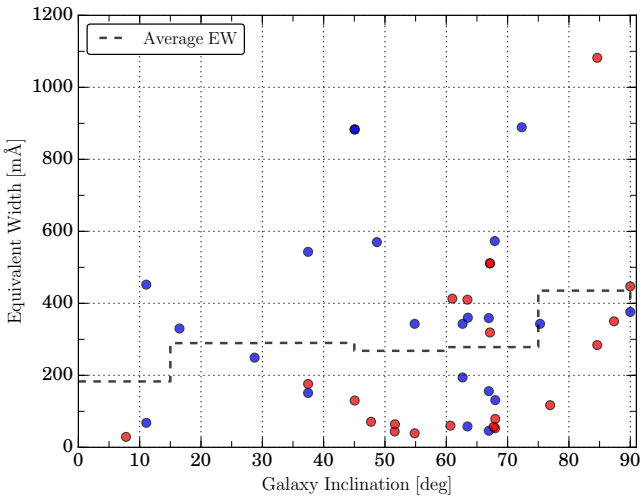

Figure 6. Equivalent width of each absorber as a function of the inclination angle of the associated galaxy. The dashed black line shows the mean EW of all absorbers in bins of 15°.

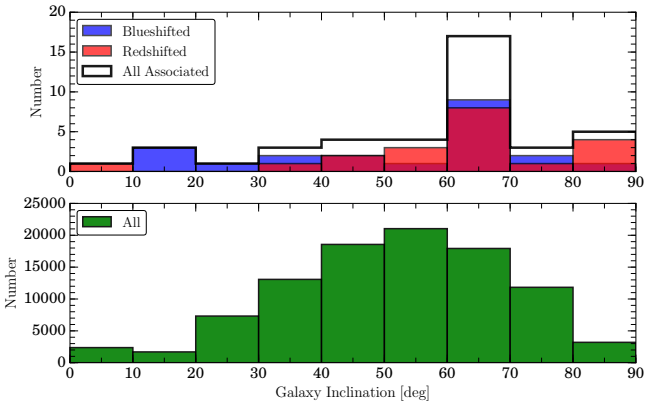

Figure 7. Top: Distribution of inclinations for all associated galaxies, split into red and blue shifted sets. **Bottom:** Distribution of inclination of all galaxies in the $cz \leq 10,000$ km/s redshift range.

It is important to note here that the majority of our sample of absorbers are measured far from galaxies (mean $\rho = 166$ kpc for blueshifted absorbers and $\rho = 261$ kpc for redshifted absorbers). Additionally, the differential velocity between galaxy and absorber (Δv) is on the order of the rotation velocity for spiral galaxies (average $\Delta v = 89$ km/s for blueshifted, $\Delta v = -134$ km/s for redshifted absorbers). Without further knowledge of the rotation velocity and orientation of each galaxy however, we can only speculate at the origins of the dichotomy between red and blue-shifted absorbers.

In total, 61% of blueshifted and 80% of redshifted absorbers are associated with high inclined galaxies ($i \geq 50$ deg). 56% of all galaxies in the survey volume are highly inclined, indicating a preference for detecting absorption around inclined galaxies. Figure 7 shows the distribution of galaxy inclinations for both the red and blue-shifted associated galaxies and all galaxies within the survey volume. Again, we tested the difference between the full distribution of inclination angles and the distribution for all (red + blue-shifted) associated galaxies with the KS and AD tests, this time yielding $p = 0.0025$. Hence, it appears that there is a significant bias towards detecting Lyα absorption around highly inclined galaxies.

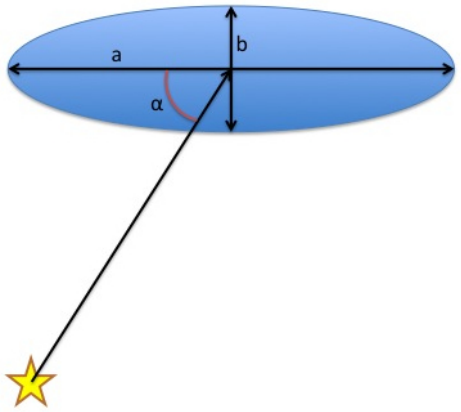

Figure 8. Azimuth is the angle, α, between the major axis of the galaxy, a, and a vector extending from the AGN target to the galaxy center.

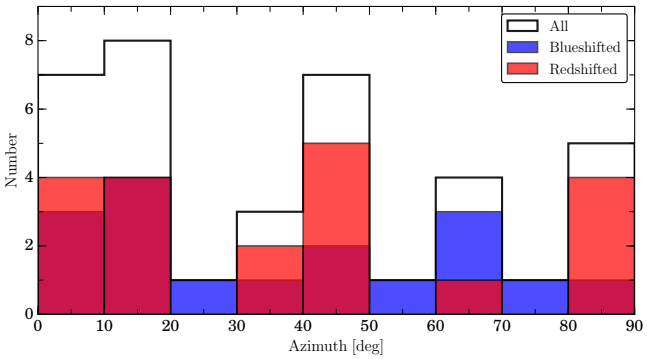

Figure 9. The distributions of azimuth angles for red and blue-shifted samples.

3.4. *Azimuth*

In this section we examine properties of absorbers as a function of their azimuthal angle with respect to their associated galaxy. Azimuth is defined as the angle between the major axis of a galaxy and the vector connecting the absorption feature and the midpoint of the galaxy plane. Figure 8 illustrates this. The mean azimuth angle for blueshifted absorbers is 37°, and 38° for redshifted absorbers. Figure 9 shows the distribution of azimuth angles for both red and blue-shifted absorbers. Unlike the findings of Kacprzak et al. (2011, 2012), who find a bimodal distribution of Mg II absorbers around galaxies, our distributions of Lyα absorbers are generally consistent with a flat, or random distribution. There is a slight overabundance of absorbers around 0° azimuth in both red and blue-shifted samples, but we cannot assign this observation much significance yet given the small sample size. We additionally find no significant correlation between azimuth angle and EW or Δv.

4. SUMMARY

We have measured 175 Lyα absorption lines in the spectra of 32 COS and 3 STIS targets. Table 3 presents a breakdown of our results when separating absorber-galaxy pairs in to red and blue-shifted samples. The fol-

Δv	# of systems	Mean EW [mÅ]	Median EW [mÅ]	Mean R_{vir} [kpc]	Mean ρ [kpc]	Mean Δv [kms^{-1}]	Mean Inc. [deg]	Mean Az. [deg]
(1)	(2)	(3)	(4)	(5)	(6)	(7)	(8)	(9)
Redshifted	20	236.8 ± 15.9	123.5 ± 9.0	210.5	260.9	-134	62	38
Blueshifted	21	353.2 ± 11.9	343.0 ± 10.0	149.1	165.5	89	53	37

Table 3
Average properties of the associated galaxy sample split into red and blue-shifted bins based on Δv.

lowing summarizes our findings:

- We introduce a likelihood parameter based on Gaussian profiles centered around ρ/R_{vir} and Δv to automate the matching of absorbers with associated galaxies.
- Of our sample of 175 Lyα absorbers, only 41 can be unambiguously paired with a single nearby galaxy using our likelihood method. 46 absorbers are located near multiple galaxies and no definitive association can be made. The remainder, over half of the total sample, are located farther than 500 kpc and 400 km/s from a galaxy.
- EW anti-correlates most strongly with ρ when normalized by R_{vir}. It follows that EW weakly correlates and anti-correlates with R_{vir} and ρ, respectively.
- The mean and maximal EW of absorbers increases with decreasing Δv. The strongest absorbers are all found within $\Delta v = \pm 100$ km/s of their associated galaxies.
- We find a dichotomy in the EW of absorption blueward vs red-ward of associated galaxies. Redshifted absorbers are weaker, with $EW = 237 \pm 16$ mÅ compared to $EW = 353 \pm 12$ mÅ for blueshifted absorbers. The difference is only significant at the 95% level, from results of both the KS and AD tests.
- Lyα absorbers are most associated with inclined galaxies. 61% of blueshifted and 80% of redshifted absorbers are associated with galaxies with $i \geq 50$ deg, whereas 56% of all galaxies in the survey volume have similarly high inclinations. The distributions of associated vs all galaxy inclinations differ at a greater than 99% significance level.
- We find no strong azimuth preference for absorption - Lyα absorbers appear to be distributed uniformly around galaxies.

REFERENCES

Carswell, B., Schaye, J., & Kim, T.-S. 2002, ApJ, 578, 43
Cen, R. 2013, ApJ, 770, 139
—. 2014, ApJ, 789, L21
Chen, H.-W., Lanzetta, K. M., Webb, J. K., & Barcons, X. 1998, ApJ, 498, 77
—. 2001, ApJ, 559, 654
Corwin, Jr., H. G., Buta, R. J., & de Vaucouleurs, G. 1994, AJ, 108, 2128
Côté, S., Wyse, R. F. G., Carignan, C., Freeman, K. C., & Broadhurst, T. 2005, ApJ, 618, 178
Danforth, C. W., & Shull, J. M. 2005, ApJ, 624, 555
—. 2008, ApJ, 679, 194
Danforth, C. W., Shull, J. M., Rosenberg, J. L., & Stocke, J. T. 2006, ApJ, 640, 716
Danforth, C. W., Keeney, B. A., Tilton, E. M., et al. 2014, ArXiv e-prints
Erb, D. K. 2008, ApJ, 674, 151
Kacprzak, G. G., Churchill, C. W., Barton, E. J., & Cooke, J. 2011a, ApJ, 733, 105
Kacprzak, G. G., Churchill, C. W., Evans, J. L., Murphy, M. T., & Steidel, C. C. 2011b, MNRAS, 416, 3118
Kacprzak, G. G., Churchill, C. W., & Nielsen, N. M. 2012, ApJ, 760, L7
Keeney, B. A., Stocke, J. T., Syphers, D., et al. 2013, in American Astronomical Society Meeting Abstracts, Vol. 222, American Astronomical Society Meeting Abstracts, 214.18
Kereš, D., & Hernquist, L. 2009, ApJ, 700, L1
Kim, T.-S., Bolton, J. S., Viel, M., Haehnelt, M. G., & Carswell, R. F. 2007, MNRAS, 382, 1657
Lanzetta, K. M., Bowen, D. V., Tytler, D., & Webb, J. K. 1995, ApJ, 442, 538
Lehner, N., Savage, B. D., Richter, P., et al. 2007, ApJ, 658, 680
Liang, C. J., & Chen, H.-W. 2014, MNRAS, 445, 2061
Lundgren, B. F., Brunner, R. J., York, D. G., et al. 2009, ApJ, 698, 819
Mathes, N. L., Churchill, C. W., Kacprzak, G. G., et al. 2014, ApJ, 792, 128
McLin, K. M., Stocke, J. T., Weymann, R. J., Penton, S. V., & Shull, J. M. 2002, ApJ, 574, L115
Meiksin, A. A. 2009, Reviews of Modern Physics, 81, 1405
Oppenheimer, B. D., & Davé, R. 2009, MNRAS, 395, 1875
Oppenheimer, B. D., Davé, R., Katz, N., Kollmeier, J. A., & Weinberg, D. H. 2012, MNRAS, 420, 829
Penton, S. V., Stocke, J. T., & Shull, J. M. 2002, ApJ, 565, 720
—. 2004, ApJS, 152, 29
Prochaska, J. X., Weiner, B., Chen, H.-W., Mulchaey, J., & Cooksey, K. 2011, ApJ, 740, 91
Prochaska, J. X., Weiner, B. J., Chen, H.-W., & Mulchaey, J. S. 2006, ApJ, 643, 680
Putman, M. E., Peek, J. E. G., & Heitsch, F. 2009a, ArXiv e-prints
Putman, M. E., Henning, P., Bolatto, A., et al. 2009b, in Astronomy, Vol. 2010, astro2010: The Astronomy and Astrophysics Decadal Survey, 241
Rudie, G. C., Steidel, C. C., & Pettini, M. 2012a, ApJ, 757, L30
Rudie, G. C., Steidel, C. C., Shapley, A. E., & Pettini, M. 2013, ApJ, 769, 146
Rudie, G. C., Steidel, C. C., Trainor, R. F., et al. 2012b, ApJ, 750, 67
Savage, B. D., Kim, T.-S., Wakker, B. P., et al. 2014, ApJS, 212, 8
Shull, J. M., Smith, B. D., & Danforth, C. W. 2012, ApJ, 759, 23
Smith, B. D., Hallman, E. J., Shull, J. M., & O'Shea, B. W. 2011, ApJ, 731, 6
Steidel, C. C., Erb, D. K., Shapley, A. E., et al. 2010, ApJ, 717, 289
Stewart, K. R., Kaufmann, T., Bullock, J. S., et al. 2011, ApJ, 738, 39
Stocke, J. T., Keeney, B. A., Danforth, C. W., et al. 2013, ApJ, 763, 148
Tejos, N., Morris, S. L., Crighton, N. H. M., et al. 2012, MNRAS, 425, 245
Tejos, N., Morris, S. L., Finn, C. W., et al. 2014, MNRAS, 437, 2017
Thom, C., Tumlinson, J., Werk, J. K., et al. 2012, ApJ, 758, L41
Tripp, T. M., Aracil, B., Bowen, D. V., & Jenkins, E. B. 2006a, ApJ, 643, L77
Tripp, T. M., Bowen, D. V., Sembach, K. R., et al. 2006b, in Astronomical Society of the Pacific Conference Series, Vol. 348, Astrophysics in the Far Ultraviolet: Five Years of Discovery with FUSE, ed. G. Sonneborn, H. W. Moos, & B.-G. Andersson, 341
Tripp, T. M., Lu, L., & Savage, B. D. 1998, ApJ, 508, 200
Tripp, T. M., Sembach, K. R., Bowen, D. V., et al. 2008, ApJS, 177, 39
Tully, R. B., Courtois, H. M., Dolphin, A. E., et al. 2013, AJ, 146, 86

Tumlinson, J., Werk, J. K., Thom, C., et al. 2011, ApJ, 733, 111
van de Voort, F., & Schaye, J. 2012, MNRAS, 423, 2991
van de Voort, F., Schaye, J., Booth, C. M., Haas, M. R., & Dalla Vecchia, C. 2011, MNRAS, 414, 2458
Wakker, B. P., Hernandez, A. K., French, D. M., et al. 2015, ApJ, 814, 40
Wakker, B. P., & Savage, B. D. 2009, ApJS, 182, 378
Werk, J. K., Prochaska, J. X., Tumlinson, J., et al. 2014, ApJ, 792, 8
York, D. G., vanden Berk, D., Richards, G. T., et al. 2005, in IAU Colloq. 199: Probing Galaxies through Quasar Absorption Lines, ed. P. Williams, C.-G. Shu, & B. Menard, 58–64